International Journal of Nanomedicine

Dovepress
open access to scientific and medical research

Open Access Full Text Article

ORIGINAL RESEARCH

Bioactive Nanocomposite Microsponges for Effective Reconstruction of Critical-Sized Calvarial Defects in Rat Model

Mohan Wang[1,2], Zheyuan Gu[2], Beibei Li[2], Jingyi Zhang[2], Lu Yang[2], Xianyu Zheng[2], Faming Pan[1], Jiacai He[1,2]

[1]Department of Epidemiology and Biostatistics, School of Public Health, Anhui Medical University, Hefei, 230032, People's Republic of China; [2]Stomatologic Hospital & College, Anhui Medical University, Key Laboratory of Oral Diseases Research of Anhui Province, Hefei, 230032, People's Republic of China

Correspondence: Jiacai He; Faming Pan, Email hejiacai@ahmu.edu.cn; famingpan@ahmu.edu.cn

Introduction: Micro-sized sponge particulates have attracted extensive attention because of their potential to overcome the intrinsic limitations of conventional monolithic scaffolds in tissue engineering. Bioactive nanocomposite microsponges are regarded as potential bone substitute materials for bone regeneration.

Methods: Based on a combination of microfluidic emulsion with further freezing and in situ thawing, chitosan (CS)-hydroxyapatite (HAP) microsponges were prepared and characterized in terms of their morphology and elemental distribution using a scanning electron microscope equipped with an X-ray detector. The swelling ratio, porosity, degradability, antibacterial activity, and bioactivity were detected and analyzed. The biological functions of the CS-HAP microsponges were examined to assess the adhesion, proliferation, and differentiation of in vitro co-cultured rat bone marrow mesenchymal stem cells (rBMSCs). Furthermore, the CS-HAP microsponges were used as cell-free scaffolds and implanted into calvarial defects in a rat model to evaluate the in vivo osteogenesis.

Results: The CS-HAP microsponges have a porous structure with high porosity (~76%), good swelling capacity (~1900%), and shape-memory properties. The results of in vitro experiments show that the CS-HAP microsponges achieve good bioactivity and promote osteogenic differentiation of rBMSCs. Furthermore, the CS-HAP microsponges significantly promote bone regeneration in rat calvarial defects.

Conclusion: The bioactive CS-HAP microsponges have the potential to be used as bone substitute materials for bone tissue engineering.

Keywords: bioactive, hydroxyapatite, chitosan, nanocomposite microsponges, bone tissue engineering

Introduction

The reconstruction of critical-sized bone defects in clinics generally uses autografts, allografts, and bone graft substitutes.[1] As the gold standard, autografts are limited by their source and donor site morbidity, while allografts are subject to infection and immune rejection.[2,3] As a result of advances in bone tissue engineering (BTE), synthetic scaffolds serving as porous matrices for tissue formation represent promising biomaterials for bone repair and regeneration.[4,5]

For BTE, porous scaffold materials play a key role in providing a favorable spatial environment for cell adhesion, migration, and differentiation.[6,7] Traditional BTE relies on three-dimensional (3D) monolithic scaffolds, which have limitations in terms of nutrient diffusion, nonuniform cell distribution, and insufficient neovascularization inside the scaffolds.[6–8] Micro-sized sponge particulates offer the advantages of high porosity, high surface area, excellent elasticity, and interstitial spaces.[9] These features overcome the intrinsic limitations of conventional 3D scaffolds.[10,11] Moreover, micro-sized particulates have excellent injectability, ensuring minimally invasive procedures.[9]

Received: 8 September 2022
Accepted: 13 December 2022
Published: 27 December 2022

© 2022 Wang et al. This work is published and licensed by Dove Medical Press Limited. The full terms of this license are available at https://www.dovepress.com/terms.php and incorporate the Creative Commons Attribution – Non Commercial (unported, v3.0) License (http://creativecommons.org/licenses/by-nc/3.0/). By accessing the work you hereby accept the Terms. Non-commercial uses of the work are permitted without any further permission from Dove Medical Press Limited, provided the work is properly attributed. For permission for commercial use of this work, please see paragraphs 4.2 and 5 of our Terms (https://www.dovepress.com/terms.php).

In our previous study, we proposed an efficient microfluidic method and fabricated uniform, injectable, shape-memory chitosan (CS) microsponges, which have no requirement for any potentially cytotoxic cross-linkers or freeze-drying process.[12] The prepared CS microsponges exhibit great advantages as cell carriers for tissue engineering, facilitating in vitro cell attachment and proliferation. Nevertheless, the high degradability and low mechanical and osteoconductive properties of CS needs to be improved to satisfy the requirements of further applications.[13–15] To address this issue, CS is often combined with a bioactive material, such as hydroxyapatite (HAP) or β-tricalcium phosphate (β-TCP), to overcome its disadvantages for BTE.[15–19] As the major inorganic component of human bone and teeth, HAP nanoparticles (nHAP) are known to promote cell adhesion, proliferation, and osteogenic differentiation, and can enhance the in vivo repair of bone tissues.[20–22] In recent years, CS-HAP composite biomaterials have been fabricated and applied for tissue engineering in the form of membranes, scaffolds, and particles.[12,18–20,23] Compared with 3D scaffolds, porous microparticles and the void spaces among them provide a 3D environment for cell adhesion, proliferation, and nutrient transfer, and can form self-assembled cell–microparticle aggregates.[9,24] Moreover, the distribution of nHAP in porous materials reduces degradability and promotes the osteoconductive properties of the composite material.[3,25,26]

In this study, uniform and porous CS-HAP nanocomposite microsponges are developed using our previously reported method.[12] The developed CS-HAP microsponges display a porous structure with high porosity, good swelling capacity, and shape-memory properties. The CS-HAP microsponges exhibit good bioactivity and promote osteogenic differentiation in in vitro rat bone marrow mesenchymal stem cells (rBMSCs). Furthermore, the CS-HAP microsponges serve as cell-free scaffolds for promoting the in vivo reconstruction of calvarial bone defects. Thus, the developed CS-HAP microsponges have great potential to be used as bone substitute materials for BTE, particularly for minimally invasive procedures and irregular bone defects.

Materials and Methods

Preparation of Nanocomposite Microsponges

The microfluidic devices have a co-axial structure consisting of an inner discontinuous phase channel (inner diameter 100 μm) and outer continuous phase channel (inner diameter 410 μm). A solution containing 1 wt.% CS (degree of deacetylation ≥ 95%, viscosity of 100–200 mPa·s) was obtained by dissolution in 2% v/v acetic acid solution. For the CS-HAP composite solution, HAP (<100 nm) was added to the CS solution and stirred to obtain a homogeneous CS-HAP solution with a weight ratio of 1:1. The obtained solution served as the discontinuous phase. The oil phase was prepared by adding Span 80 to cyclohexane with a total emulsifier content of 3% (w/v). Toluene was placed in a beaker and kept between −40°C~−20°C in a bath filled with liquid nitrogen. CS-HAP droplets were collected from the microfluidic devices with the solidification bath, then treated with pre-cooled NaOH ethanol solution (0.1 M) at −10°C. The obtained CS-HAP microsponges were washed adequately and collected for subsequent experiments. Figure 1 shows the scheme used to prepare the porous CS-HAP microsponges.

Examination of Morphology, Elemental Composition and Distribution

The morphological, surface, and porous structures of the CS-HAP microsponges were investigated using an optical microscope (OPM; Leica DM2700P, Germany) and a scanning electron microscope (SEM; Zeiss Supra 40, Germany). The phase composition of nHAP was characterized by an X-ray diffractometer (XRD; Philips X'Pert PRO SUPER, Netherlands) with Cu Kα radiation. The elemental composition and distribution of the CS-HAP surface were measured by energy-dispersive X-ray spectroscopy (EDX) using an SEM equipped with an X-ray detector (Oxford Instruments, Ultim Max, UK).

Evaluation of Porosity, Swelling Ratio and Degradation of Scaffolds

The porosity and swelling ratio of the CS-HAP microsponges were measured in a previous study.[12,27] We roughly estimated these quantities because the small microsponges were difficult to weigh. CS-HAP macroscopic scaffolds were prepared by lyophilizing the CS-HAP solution with the same concentration, then treating with 0.1 M NaOH ethanol solution. The dried scaffolds were measured as W_1 prior to immersion in absolute ethanol for 4 h. The macroscopic

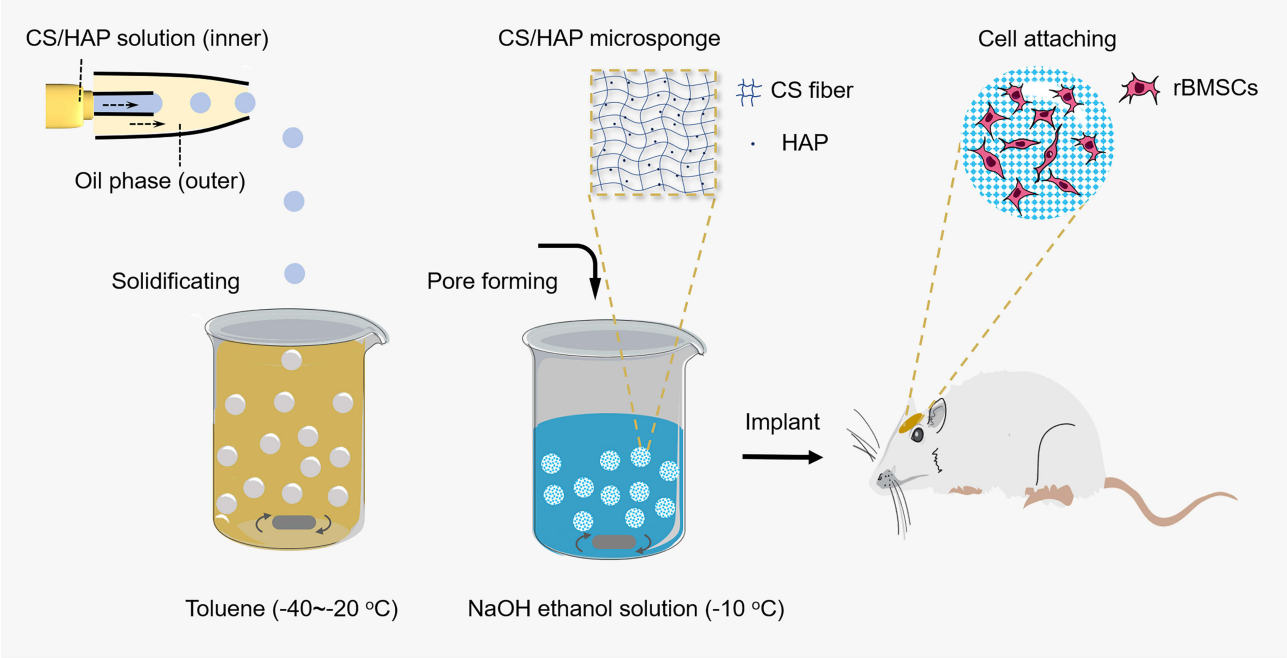

Figure 1 Schematic representation of preparation method and application of bioactive CS-HAP nanocomposite microsponges.

scaffolds were weighed as W_2 after removing the surface ethanol with filter paper. The porosity analyses were performed in five replicates, with the porosity calculated as:

Porosity (%) = $[(W_2 - W_1)/\rho V] \times 100$ (1)

where ρ represents the density of absolute ethanol and V represents the volume of the sample.

For the swelling ratio, the dried scaffolds were weighed as $W_{d,}$ and then submerged in water for a set period of time. Each sample was weighed as W_s after removing the extra water with filter paper. The tests were conducted three times and the swelling ratio was evaluated as:

Swelling ratio (%) = $[(W_s - W_d)/W_d] \times 100$ (2).

The CS-HAP microsponges were immersed in 0.1 M saline buffer phosphate (PBS; pH = 7.4) containing 1.5 mg/mL lysozyme to evaluate their degradability, following our previous method.[12] At the predetermined time points, the CS-HAP microsponges were collected and observed under the OPM.

Vitro Bioactivity in Simulated Body Fluid

Simulated body fluid (SBF) was prepared to evaluate the in vitro bioactivity of the CS-HAP microsponges according to Kokubo's method.[28] The CS-HAP microsponges were soaked in SBF solution (5 mL) and incubated at 37°C for 1, 4, and 7 days, and the SBF solution was renewed every 48 h. The CS-HAP microsponges were gently washed with distilled water to remove the SBF solution and freeze-dried at −50°C for 12 h. The elemental compositions of calcium and phosphate were measured using energy-dispersive X-ray spectroscopy (EDS) coupled with the SEM (SEM-EDS) (Oxford Ultim Max, UK).

Antibacterial Capacity Test

The antibacterial capacity of the prepared CS microsponges and CS-HAP microsponges was tested against *Staphylococcus aureus (S. aureus)* and *Escherichia coli (E. coli)* using the growth turbidity method.[27] First, the bacteria were cultured overnight in a broth medium. The turbidities were adjusted to 1–2 × 10^8 CFU/mL with the MacFarland 0.5 standard at 625 nm. Subsequently, 100 μL of the diluted bacterial suspension with 150 mg of the tested microsponges was inoculated into 10 mL of the broth medium, and then incubated at 37°C and shaken (150 rpm) for 18 h. An untreated bacterial suspension was used as a control. The optical densities (OD) of the bacterial suspension at 600 nm were

measured using a microplate reader (Tecan Infinite 200 Pro, Switzerland) to evaluate the antibacterial capacity. Both tests were conducted with five replications. The percentage of bacterial growth inhibition was calculated according to:

$$\text{Bacterial growth inhibition (\%)} = [(OD_c - OD_t)/OD_c] \times 100 \quad (3)$$

where OD_c and OD_t represent the mean OD of the control and treated samples, respectively.

A live/dead staining assay was also taken to evaluate the antibacterial capacity of the CS and CS-HAP microsponges. Briefly, *S. aureus* and *E. coli* were cultured to the post-log phase, and equal weights of materials were added to 1 mL of resuspended bacteria solution (diluted 1000 times). The suspension was then centrifuged at 6000 rpm for 3 min and suspended in 50 μL physiological saline after being incubated for 4 h at 37°C. Next, the bacteria were stained with a live/dead staining kit (Invitrogen, USA) for 15 min. Finally, the samples were observed through a fluorescent microscope to distinguish dead bacteria (red staining) from live bacteria (green staining).

Cell Isolation and Culture

The rBMSCs were collected and cultured from the tibia and femur of 4-week-old male Sprague–Dawley (SD) rats. The tibia and femur bones were washed several times in PBS. The midshaft bone marrow of the tibia and femur was flushed out, suspended, and cultured in alpha-minimum essential medium (α-MEM) (Hyclone, USA) containing 20% fetal bovine serum (FBS; Corning, USA), 100 U/mL penicillin, and 100 U/mL streptomycin in an incubator with 5% CO_2 at 37°C. When 70%–80% confluence was reached, the rBMSCs were passaged using a 0.25% trypsin-EDTA solution. The cells obtained at passage 3 were used in subsequent experiments.

Cell Adhesion and Viability on Scaffolds

The cytotoxicity of the CS-HAP microsponges was examined using a CCK-8 assay (Dojindo, Kumamoto, Japan). Briefly, 1×10^4 rBMSCs with 1×10^2 microsponges were seeded in a 96-well plate for co-culturing. Five replications were performed for each group. After 1, 4, and 7 days of co-culturing, the culture medium was discarded. Then, 100 μL of working solution (10% CCK-8 solution in α-MEM) was added and incubated at 37°C for 2 h. Subsequently, the supernatant was collected and the OD value was measured at 450 nm. The samples were collected and a live/dead assay was conducted (Dojindo, Kumamoto, Japan) following the manufacturer's instructions. Confocal images were obtained by confocal laser scanning microscopy (CLSM; Zeiss LSM 880, Germany). Green fluorescence indicated live cells. Red fluorescence indicated dead cells.

Cell attachment tests were conducted according to our previous work.[12] For this, a 20-mL suspension of rBMSCs was mixed with CS-HAP microsponges at a quantity ratio of 100:1. The number of rBMSCs in 1 mL of the suspension was identified as C_0. At a predetermined point, 1 mL of the mixed suspension was harvested and the unattached cells were counted as C_t. The adhesion efficiency was calculated as $(C_0 - C_t)/C_0 \times 100\%$. To further observe the morphology of cell attachment and proliferation, the cell nucleus was stained with 4, 6-diamino-2-phenyl indole (DAPI), and the cytoskeleton was stained with phalloidin (Sigma-Aldrich, USA). Confocal images were obtained by CLSM. Furthermore, the samples were lyophilized and the cell distribution and morphology were observed by SEM.

Real-Time Polymerase Chain Reaction Assays

The 2×10^5 rBMSCs with 2×10^3 CS microsponges were co-cultured in 6-well plates. After 14 days of incubation, the cells were digested by a 0.25% trypsin-EDTA solution and collected. The total RNA was extracted using TRIzol (Sigma-Aldrich, USA). Immediately, complementary DNA (cDNA) synthesis of the extracted mRNA was performed using the PrimeScript RT Kit (Takara, Japan). The synthesized cDNAs were used for real-time polymerase chain reaction (RT-PCR) analysis using the SYBR premix Ex Taq (Takara, Japan). A 20-μL reaction system was created using Stratagene Mx3000p (Agilent Technologies, USA). The C_t values of the sample were analyzed by the $2^{-\Delta\Delta Ct}$ method.

Alkaline Phosphatase Staining and Activity

The 1×10^5 rBMSCs were seeded in 6-well plates and co-cultured with microsponges using the Transwell apparatus. After 14 days of culturing in an osteogenic medium, each group was fixed with 4% paraformaldehyde at room temperature for 30 min and washed twice using PBS, then incubated with an alkaline phosphatase (ALP) kit (Beyotime, China) in the

dark for 2 h. The cells were washed three times with PBS and observed under the OPM. Furthermore, an ALP assay kit (Beyotime, China) was used to analyze the ALP activity following the manufacturer's instructions. OD was measured at 405 nm using a microplate reader.

Animal Surgery of Critical-Sized Calvarial Defects in Rat Model

All animal studies were approved by the Independent Ethics Committee of Anhui Medical University (Approval number: LLSC20170177), and were performed in accordance with the "Guide for the Care and Use of Laboratory Animals." A total of 18 male SD rats (250–300 g) were purchased from the Animal Experiment Center of Anhui Medical. The calvarial defect model was conducted following a previously described method.[29] Briefly, the animals were anesthetized with 4% chloral hydrate by intraperitoneal injection, then a sagittal incision was made along the skull. Full-thickness flaps were raised to expose the calvarium. A 5-mm bone defect was made in the middle of the skull using a trephine. The bone defects were randomly divided into three groups, each containing six animals. In the two experimental groups, the bone defects were filled with the CS and CS-HAP scaffolds, respectively; in the control group, the bone defects were not filled with any material. The incisions were closed with 3–0 silk sutures. The animals were intramuscularly injected with antibiotics for three consecutive days. After a healing period of 12 weeks, the animals were sacrificed with an overdose of pentobarbital. The rat calvaria were harvested for further analyses.

Micro-Computed Tomography Analysis of Bone Defects

The calvarial specimens were fixed in paraformaldehyde and scanned by microcomputed tomography (micro-CT; AX2000, China) with scanning parameters of 80 kV and 100 μA, an exposure time of 500 ms, and a resolution of 15 μm. The 3D images were then reconstructed and analyzed using the VG Studio Max 3.4 software (VG Studio MAX, Heidelberg, Germany). The bone volume/total volume (BV/TV), trabecular number (Tb. N), and trabecular separation (Tb. Sp) values were used to evaluate the new bone formation.

Histological Assessment

The specimens were decalcified in 10% EDTA–2Na and embedded in paraffin. A series of 6-μm-thick sections was prepared and stained with hematoxylin-eosin (H&E), Goldner, and immunohistochemical staining according to standard protocols. The acquired slices were histomorphometrically examined with the OPM.

Statistical Analysis

All experiments were performed in triplicate, unless otherwise specified. The quantitative data are presented as mean ± standard deviation (s.d.), and were processed using SPSS version 17.0.1 (SPSS Inc., Chicago, IL, USA). Tukey's post-hoc test for independent samples was used for comparisons between two groups, and analysis of variance (ANOVA) was applied for three or more groups.

Results and Discussion

Material Preparation and Characterization

The morphology of the emulsified CS-HAP droplets was observed under the OPM, showing that the spherical droplets with uniform size were well-dispersed in aqueous solution (Figure 2A). The pre-cooled toluene solution was prepared to solidify the droplets, and micro-sized ice crystals were observed to be randomly distributed over the whole droplets. After the droplets had been treated with pre-cooled NaOH ethanol solution to melt the ice crystals in the solid microspheres, the porous structures of the CS-HAP microsponges were obtained, as shown in Figures 2B and C. Subsequently, the microstructures of the CS-HAP microsponges were observed by SEM after lyophilization (Figure S1). SEM images with different magnifications suggest that the microsponge surface has a random network of pores measuring several micrometers (Figures 2D–F and S2); the white arrows in Figure 2F represent nHAP. XRD analysis verified the incorporation of HAP in the CS-HAP composite microsponges. The XRD peaks are a very good match with the JCPDS standard XRD card No. 86–1199 for HAP (Figure 2G).

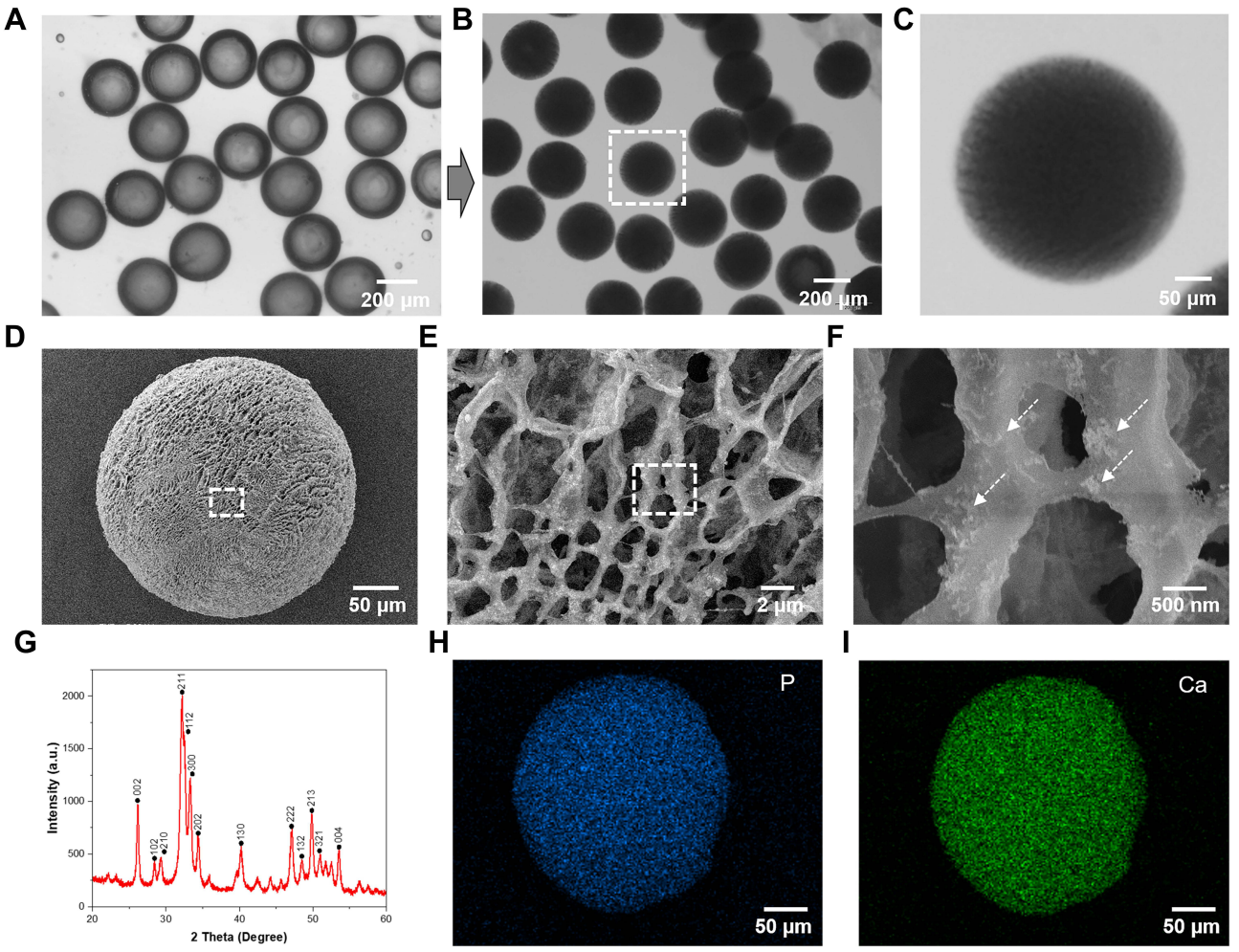

Figure 2 Material characterizations of CS-HAP microsponges. (**A–C**) OPM images of uniform CS-HAP droplets and porous CS-HAP microsponges. (**D–F**) SEM images showing the morphology of porous-structured CS-HAP microsponges at different magnifications (white arrows represent nHAP in (**F**)). (**G**) XRD pattern of HAP nanoparticles. (**H** and **I**) SEM-EDX mapping images revealing the distribution of P and Ca on microsponge surface.

Elemental mapping performed by SEM-EDX indicates that there is a uniform distribution of phosphorus and calcium on the microsponge surface (Figures 2H and I).

The porosity of the CS-HAP scaffolds was evaluated as ~76%, which is lower than that of the CS microsponges (~84%) prepared by the same method.[12] This decrease in porosity may relate to the addition of HAP in the polymer matrix.[30] The microsized sponges with a porous structure facilitate cell attachment and promote the transfer of oxygen and nutrients.[9] Moreover, the porous structure is favorable for elastic deformation. The shape-memory property of the CS-HAP microsponges ensures simple implementation and minimal invasiveness.[31] The photographs in video S1 show that the CS-HAP microsponges can withstand external pressure from tweezers, and rapidly recover to almost their initial shape after the pressure is removed. The porous sponge-like structure and impressive shape-memory property contribute to the swelling behavior.[27] The swelling ratio of the CS-HAP scaffolds was calculated to be as high as ~1900% (Figure S3). The volume of the lyophilized microsponges increases after immersion in water for 30 min (Figure S4). The slight expansion of the microsponges could be beneficial to the dense filling of scaffolds in bone defects. The CS-HAP microsponges undergo very slow in vitro degradation (Figure S5). Compared with the CS microsponges,[12] the introduction of HAP seems to delay the degradation process. This property is expected to facilitate new in vivo bone integration by providing more permanent structural support.

Vitro Bioactivity in SBF

The formation of bone-like apatite on the surface of BTE scaffolds is important for bone regeneration, producing bonding to the native bone tissue and facilitating osteoblast adhesion and proliferation.[32] The bioactivity of biomaterials can be estimated by in vitro mineralization in an SBF medium to predict the in vivo bone bioactivity and regeneration ability.[33] After 1, 4, and 7 days of immersion in SBF, the morphology of the mineralized crystals was observed by SEM. Mineralized crystals were formed on the surface of the CS-HAP microsponges, and the amount of the crystals obviously increased over time (Figures 3A and B). The Ca/P ratio of the CS-HAP microsponges was calculated by SEM–EDS analysis, and was found to increase continuously over time (Figure 3C). This tendency is in good agreement with the SEM observations. This increase in Ca/P ratio over mineralization time might be caused by HCO_3^- in the SBF. The existence of HCO_3^- may lead to the deposition of carbonated HAP on the CS-HAP microsponge surface.[34] The increased Ca/P ratio and formation of bone-like apatite on the surface indicates that the CS-HAP microsponges have good bioactivity, helping to ensure integrity with in vivo native bone.[32,33]

Antimicrobial Activity and Biocompatibility of Scaffolds

CS has good biodegradability, biocompatibility, and antimicrobial activity, making it an attractive biomaterial for tissue engineering.[17] To investigate whether the addition of HAP influences the antimicrobial activity, the growth turbidity of *S. aureus* and *E. coli* co-cultured with both the CS and CS-HAP microsponges was calculated. As shown in Figure 4A, both the CS and CS-HAP microsponges effectively inhibit the bacterial growth and exhibit similar bacterial growth inhibition ratios. There was no significant change in antimicrobial activity after integrating HAP, which is consistent with previous results.[35] The live/dead staining of *E. coli* and *S. aureus* further confirmed the results of the growth turbidity

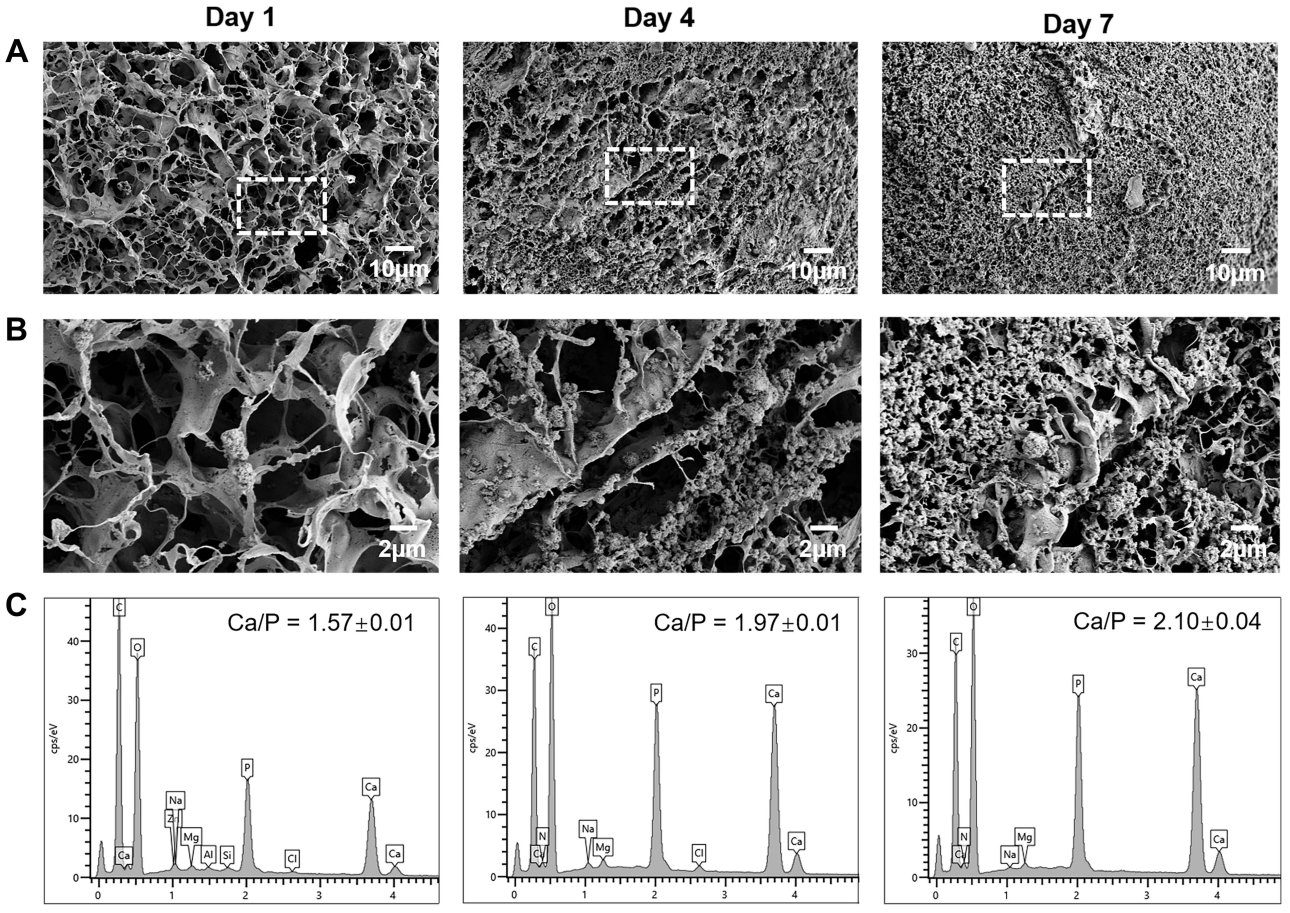

Figure 3 In vitro bioactivity of the CS-HAP microsponges in SBF after 1, 4, and 7 days. (**A**) Low magnification of SEM images of mineralized CS-HAP microsponges. (**B**) High magnification of SEM images of mineralized CS-HAP microsponges. (**C**) Evaluation of the molar ratio of Ca/P by EDS.

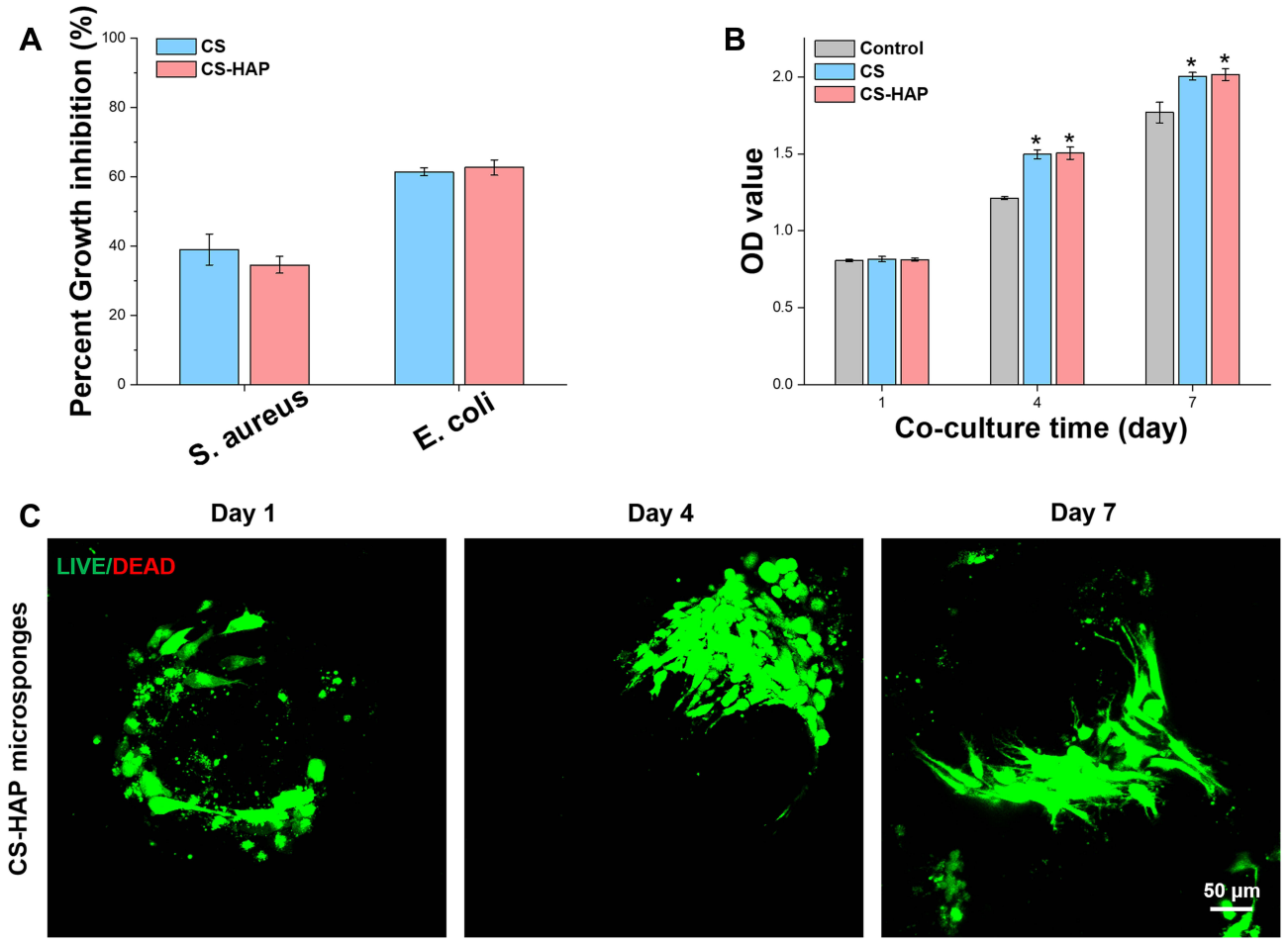

Figure 4 Bacteria and cell response to CS-HAP microsponges. (**A**) Bacterial growth inhibition of the CS and CS-HAP microsponges. (**B**) Cell viabilities by CCK-8 assay after 1, 4, and 7 days. (**C**) CLSM images of live/dead morphology of rBMSCs co-cultured with CS-HAP microsponges after 1, 4, and 7 days. *P value < 0.05 compared with the control group.

(Figure S6). The large difference in the antimicrobial activity of CS and CS-HAP microsponges against *S. aureus* and *E. coli* can be explained by the different susceptibility of gram-negative and gram-positive bacteria to CS.[36]

For the in vitro biocompatibility evaluation, the CCK-8 assay was used to estimate the biocompatibility of CS-HAP microsponges. Figure 4B shows that the number of cells increased over time. The cell proliferation increased significantly on days 4 and 7 in the CS and CS-HAP groups, compared with the control group. This can be explained by the porous structure and rough surface facilitating cell attachment, proliferation, and extracellular matrix (ECM) production.[9,12] Moreover, the void spaces among the CS-HAP microsponges provide micrometer-sized pockets for cellular invasion and proliferation.[9] The results of the live/dead assay suggest that the cells remained viable and exhibited a good cell morphology within 7 days of culture (Figure 4C). These results demonstrate the good biocompatibility of the CS-HAP microsponges.

Cell Attachment, Proliferation and Morphology on Scaffolds

One challenge faced by scaffold materials in BTE is providing adequate space for cell attachment, proliferation, and differentiation.[37] The porous CS-HAP microsponges developed in this study are expected to promote cell adhesion and proliferation. As shown in Figure S7, the cell adhesion efficiency increased continuously after cell seeding. Almost 80% of the cells adhered to the CS-HAP microsponges, similar to the percentage of CS microsponges.[12] The morphology of cell attachment and proliferation was further observed using CLSM. The CLSM images show that rBMSCs attach to and on the CS-HAP microsponges over the culture time. After 7 days of co-culturing, there is a remarkably high intensity of

red and blue fluorescence on and among the CS-HAP microsponges (Figure 5A). Cell filopodia are tightly connected with the CS-HAP microsponges. SEM was used to visualize the morphology of the rBMSCs on the CS-HAP microsponges (Figure 5B). The cells were found to be firmly attached to the surface, and elongated into a spindle-like structure within 4 days of co-culturing. On day 7, the rBMSCs extended more filopodia and connected nearby microsponges together, resulting in self-assembled cell–microsponge aggregates (Figure 5B), in line with the concept of bottom-up organization.[38] These results indicate that the CS-HAP microsponges are suitable for cell attachment and proliferation when transplanted to bone defects.

In vitro Osteogenic Differentiation Analysis

To investigate the effects of the added HAP on osteogenic differentiation, we used RT-PCR to measure the expression of two osteogenic markers: bone morphogenetic protein 2 (BMP-2) and runt-related transcription factor 2 (Runx2). The BMP-2 and Runx2 gene expressions in the CS group and the CS-HAP group were found to be significantly upregulated compared with the control group, and the expressions of BMP-2 and Runx2 in the CS-HAP group were significantly higher than in the CS group (Figures 6A and B). These results indicate that CS can be used alone or incorporated with HAP to promote bone regeneration, and the existence of HAP enhances the expression of osteogenic genes compared with pure CS.[13]

To further confirm the in vitro osteogenic potential of the scaffolds, the ALP activity of rBMSCs on day 14 was investigated. As shown in Figures 6C–E, quantitative analysis of ALP activity and ALP staining illustrate similar tendencies as for the expression of osteogenic genes. These excellent osteogenic differentiation results for rBMSCs indicate that the CS-HAP microsponges are promising bone substitute materials for further BTE applications.

Animal Experiment Histological Analysis and Evaluation

A bioactive scaffold with an ideal microstructure is vital in inducing the infiltration of stem cells and promoting tissue regeneration by recruiting the surrounding BMSCs, rather than preload cells. Scaffolds with rough and porous structures can facilitate cell adhesion, proliferation, osteogenic differentiation, and bone regeneration.[6,22,39] To investigate the potential of the CS-HAP microsponges for in vivo bone regeneration, the CS and CS-HAP microsponges were implanted as cell-free scaffolds into calvarial bone defects in rats. After 12 weeks of healing, the newly formed bone was analyzed

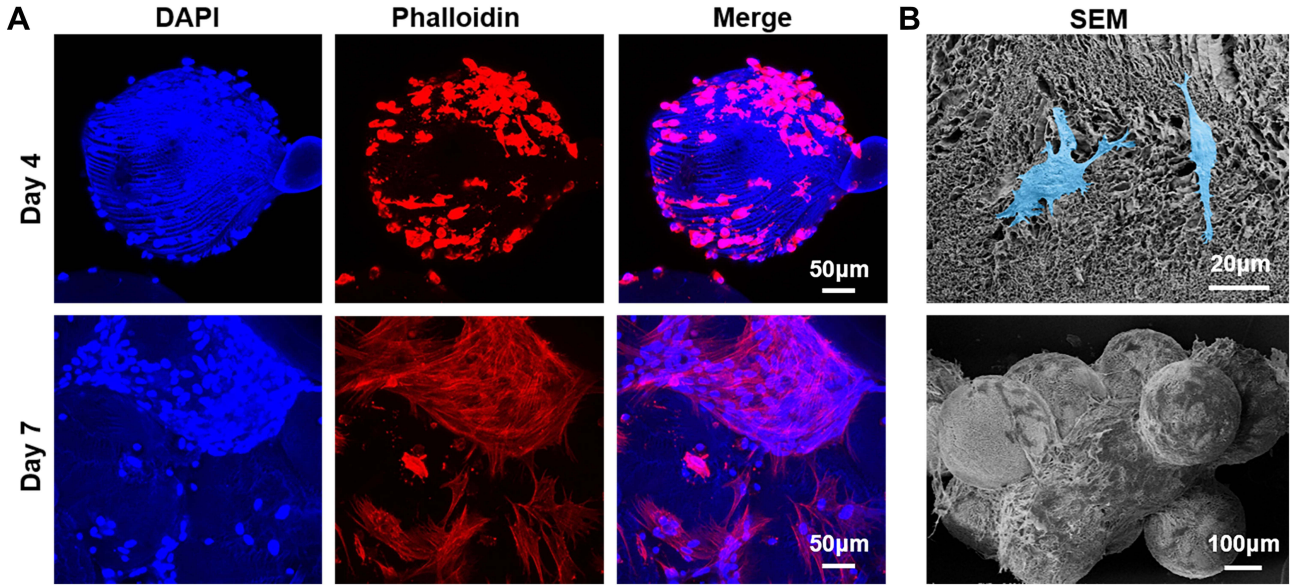

Figure 5 Cell attachment, proliferation, and morphology. (**A**) Phalloidin/DAPI staining of rBMSCs seeded on the CS-HAP microsponges after 4 and 7 days of culturing (phalloidin: red, DAPI: blue). (**B**) SEM images showing rBMSCs (marked by pseudo-color) adhered on the surface of CS-HAP microspheres after culturing for 4 and 7 days.

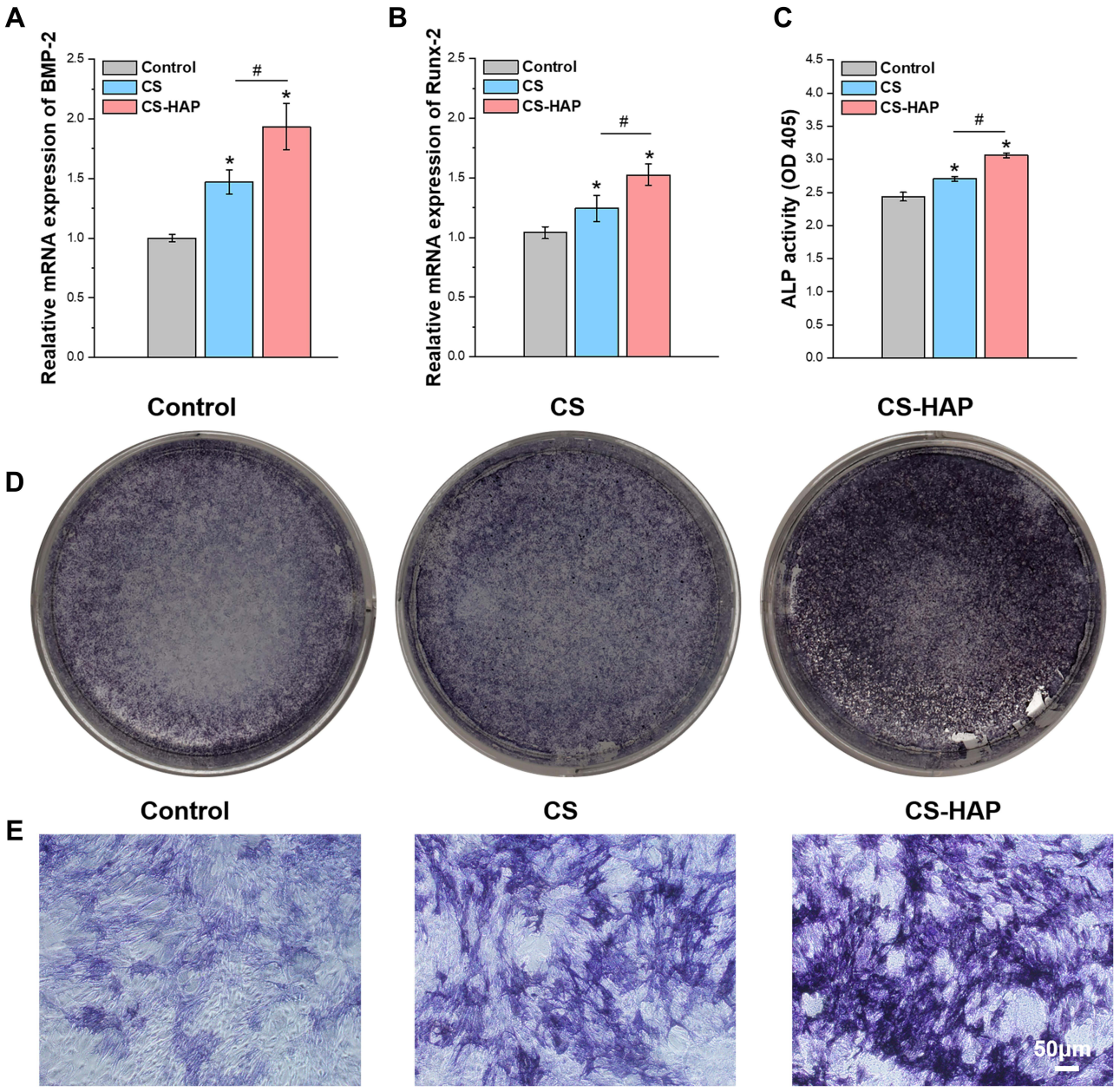

Figure 6 Osteogenic differentiation in rBMSCs. (**A** and **B**) Expression of BMP-2 and Runx2 mRNA in rBMSCs at the predetermined time. (**C**) Quantitative analysis of ALP activity. (**D** and **E**) Digital photographs and OPM images of the ALP staining of rBMSCs after 14 days of culturing. *P value < 0.05 compared with the control group; #P < 0.05 compared with the CS group.

by micro-CT with 3D reconstructions and 2D slice images (Figure 7A). The quantitative analysis demonstrates that BV/TV and Tb. N are significant higher in the CS and CS-HAP groups than in the control group, and the values in the CS-HAP group are significantly higher than in the CS group (Figures 7B and C); Tb. Sp is relatively low in all groups (Figure 7D).

To confirm the micro-CT results, H&E, Goldner, and immunohistochemical staining were conducted to assess the new bone formation. The histological results (Figure 8) show that the CS-HAP group exhibits more organized and mineralized bone tissue than the CS group and control group. This is mainly because the CS-HAP group has support materials for cell proliferation and temporary structural support for tissue ingrowth. Moreover, the slow degradation rate and osteoconductive property of CS-HAP microsponges contribute to bone formation in the bone defects. The immunohistochemical staining of representative osteogenic-related gene markers including osteopontin (OPN) and BMP-2 was performed to obtain insights into the osteogenic effects. The

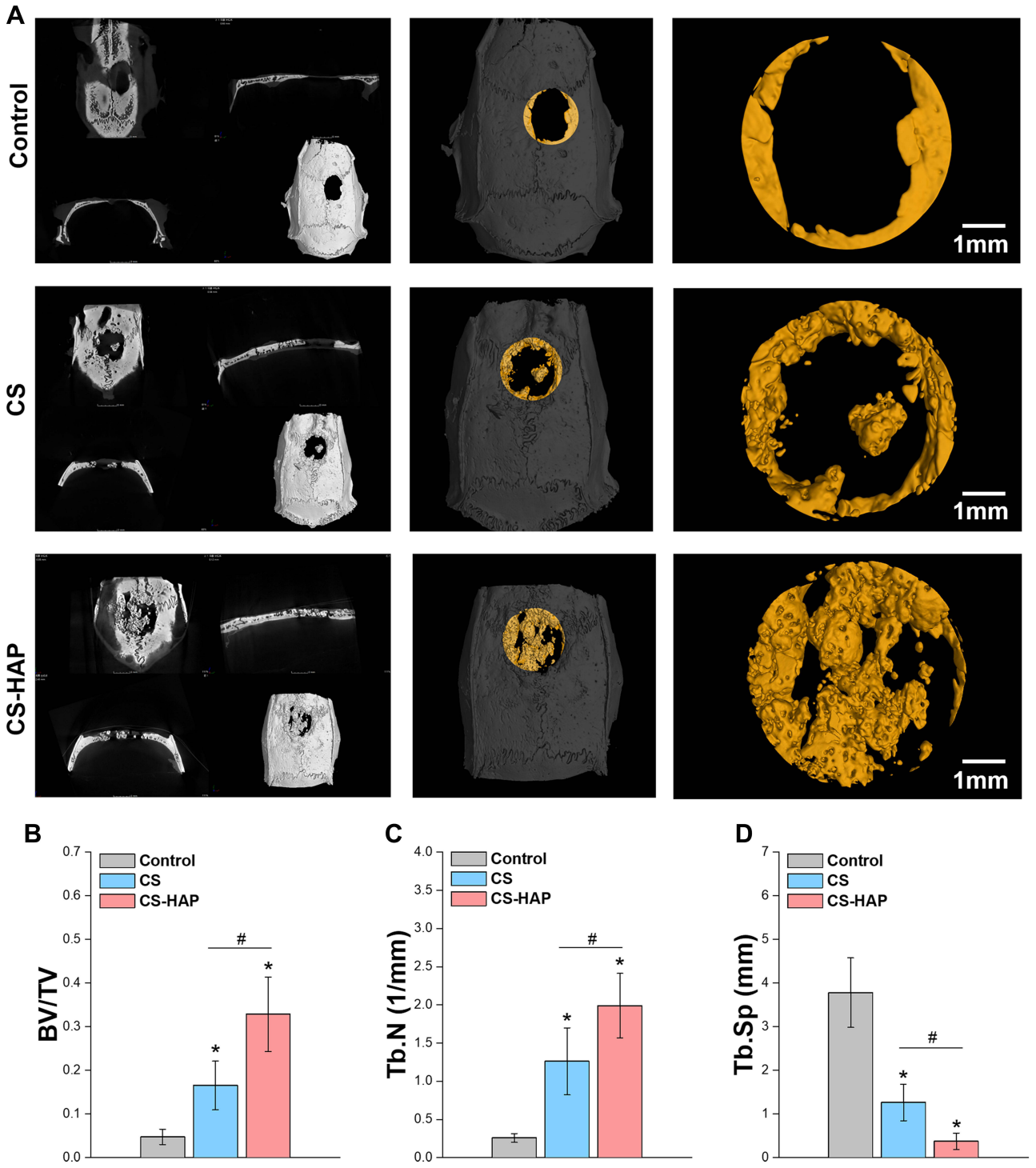

Figure 7 Micro-CT analyses of bone regeneration in rat calvarial defects. (**A**) 3D reconstructions and 2D slice images of micro-CT of the specimens after treatment for 12 weeks. (**B–D**) Quantitative comparisons of BV/TV, Tb. N, and Tb. Sp of the newly formed bone. * *P* value < 0.05 compared with the control group; #*P* < 0.05 compared with the CS group.

expressions of OPN and BMP-2 were higher than in the control group (Figure S8). The histological results further indicate that the existence of HAP promotes the osteogenic differentiation of rBMSCs and bone formation, in agreement with earlier findings.[3] Based on the above results, CS-HAP promotes new bone formation for the reconstruction of critical-sized calvarial defects in rats.

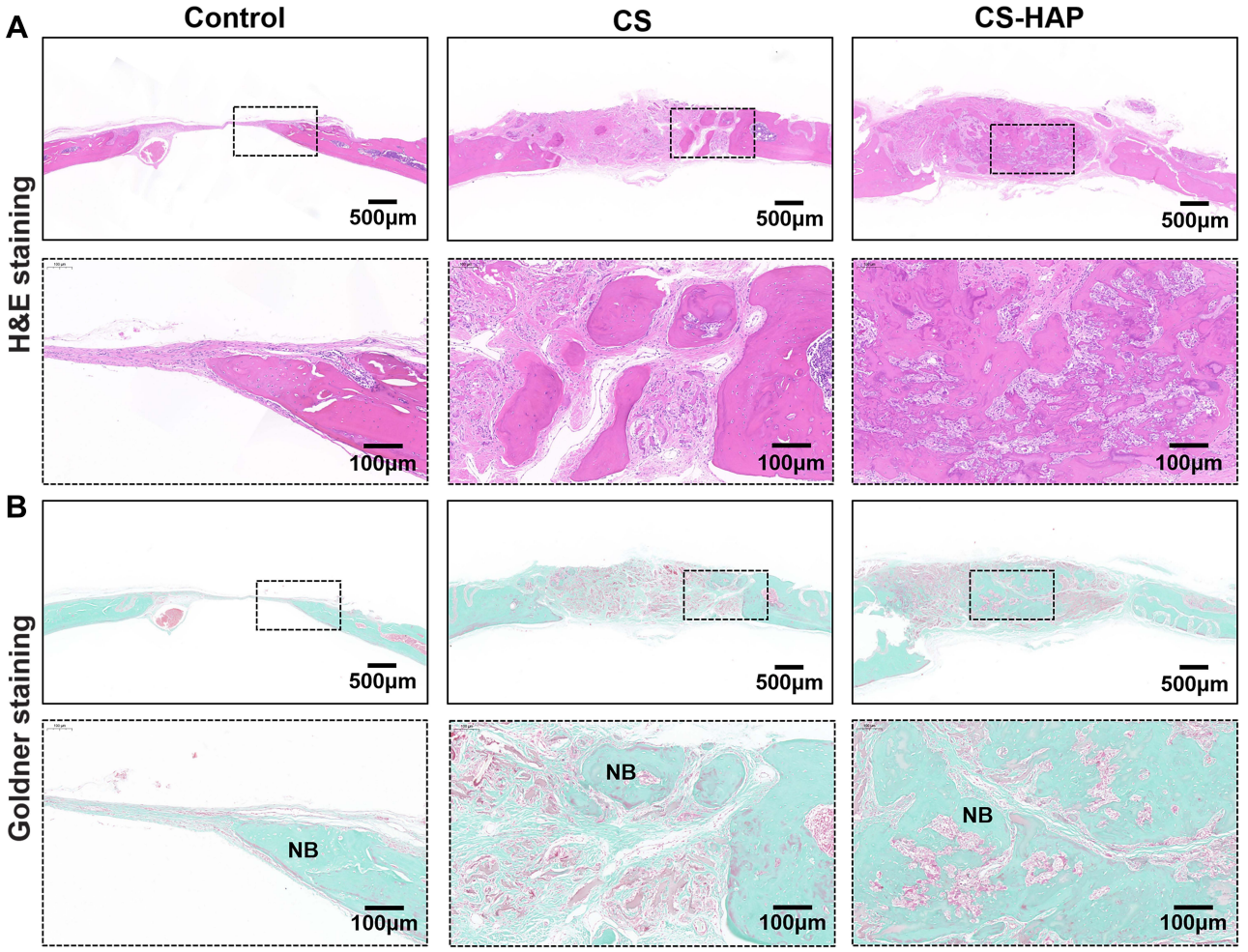

Figure 8 Histological observation of decalcified sections stained with H&E staining and Goldner staining. (**A**) H&E staining. (**B**) Goldner staining. Green indicates mineralized bone, Orange-red indicates osteoid tissue, blue-gray indicates cell nuclei.
Abbreviation: NB, new bone.

Conclusions

Bioactive nanocomposite microsponges have been successfully synthesized through microfluidic emulsion with further freezing and in situ thawing. The porous CS-HAP microsponges exhibit good in vitro biocompatibility and bioactivity, contributing to enhancing cell attachment and proliferation, and promoting osteogenic differentiation of rBMSCs. Moreover, the shape-memory characteristics and large swelling ratio of the CS-HAP microsponges are very conducive to applications concerning irregular bone defects, such as tooth extraction fossa and maxillary sinus in stomatology. The slow degradation rate in the process of in vivo osteogenesis may act to improve the quality of the newly formed bone and reduce the healing time. In summary, the CS-HAP microsponges developed in this study are promising bone substitute materials for BTE applications.

Acknowledgments

The authors thank the Center for Scientific Research of Anhui Medical University for valuable help in our experiments.

Funding

J.C. He was supported by the National Natural Science Foundation of China (81771117). X.Y. Zheng was supported by the Scientific Research Funding of Anhui Province Health Commission (AHWJ2021b152). M.H. Wang was supported by the Scientific Research Fund of Anhui Medical University (2022xkj018).

Disclosure

The authors declare no conflicts of interest.

References

1. Park HC, Son YB, Lee SL., et al. Effects of osteogenic-conditioned medium from human periosteum-derived cells on osteoclast differentiation. *Int J Med Sci*. 2017;14(13):1389–1401. doi:10.7150/ijms.21894
2. Hu B, Li Y, Wang M, et al. Functional reconstruction of critical-sized load-bearing bone defects using a Sclerostin-targeting miR-210-3p-based construct to enhance osteogenic activity. *Acta Biomater*. 2018;76:275–282. doi:10.1016/j.actbio.2018.06.017
3. Yang M, Zhou G, Castano-Izquierdo H, Zhu Y, Mao C. Biomineralization of natural collagenous nanofibrous membranes and their potential use in bone tissue engineering. *J Biomed Nanotechnol*. 2015;11(3):447–456. doi:10.1166/jbn.2015.2038
4. Thrivikraman G, Athirasala A, Twohig C, Boda SK, Bertassoni LE. Biomaterials for craniofacial bone regeneration. *Dent Clin North Am*. 2017;61(4):835–856. doi:10.1016/j.cden.2017.06.003
5. Cai L, Xu D, Chen H, Wang L, Zhao Y. Designing bioactive micro-/nanomotors for engineered regeneration. *Eng Regen*. 2021;2:109–115.
6. Jiang S, Wang M, He J. A review of biomimetic scaffolds for bone regeneration: toward a cell-free strategy. *Bioeng Transl Med*. 2021;6(2):e10206. doi:10.1002/btm2.10206
7. Koons GL, Diba M, Mikos AG. Materials design for bone-tissue engineering. *Nat Rev Mater*. 2020;5(8):584–603.
8. Yin S, Zhang W, Zhang Z, Jiang X. Recent advances in scaffold design and material for vascularized tissue-engineered bone regeneration. *Adv Healthc Mater*. 2019;8(10):e1801433. doi:10.1002/adhm.201801433
9. Daly AC, Riley L, Segura T, Burdick JA. Hydrogel microparticles for biomedical applications. *Nat Rev Mater*. 2020;5(1):20–43. doi:10.1038/s41578-019-0148-6
10. Zhang H, Jin Y, Chi C, et al. Sponge particulates for biomedical applications: biofunctionalization, multi-drug shielding, and theranostic applications. *Biomaterials*. 2021;273:120824. doi:10.1016/j.biomaterials.2021.120824
11. Leferink A, Schipper D, Arts E, et al. Engineered micro-objects as scaffolding elements in cellular building blocks for bottom-up tissue engineering approaches. *Adv Mater*. 2014;26(16):2592–2599. doi:10.1002/adma.201304539
12. Yang L, Cong Y, Zhang J, et al. Efficient fabrication of uniform, injectable, and shape-memory chitosan microsponges as cell carriers for tissue engineering. *ACS Appl Polym Mater*. 2022;4(3):1743–1751. doi:10.1021/acsapm.1c01587
13. Balagangadharan K, Dhivya S, Selvamurugan N. Chitosan based nanofibers in bone tissue engineering. *Int J Biol Macromol*. 2017;104(Pt B):1372–1382. doi:10.1016/j.ijbiomac.2016.12.046
14. Brun P, Zamuner A, Battocchio C, et al. Bio-functionalized chitosan for bone tissue engineering. *Int J Mol Sci*. 2021;22(11):5916. doi:10.3390/ijms22115916
15. Lavanya K, Chandran SV, Balagangadharan K, Selvamurugan N. Temperature- and pH-responsive chitosan-based injectable hydrogels for bone tissue engineering. *Mat Sci Eng C-Mater*. 2020;111:110862. doi:10.1016/j.msec.2020.110862
16. Hasan A, Waibhaw G, Tiwari S, Dharmalingam K, Shukla I, Pandey LM. Fabrication and characterization of chitosan, polyvinylpyrrolidone, and cellulose nanowhiskers nanocomposite films for wound healing drug delivery application. *J Biomed Mater Res A*. 2017;105(9):2391–2404. doi:10.1002/jbm.a.36097
17. Jiang SJ, Wang MH, Wang ZY, et al. Radially porous nanocomposite scaffolds with enhanced capability for guiding bone regeneration in vivo. *Adv Funct Mater*. 2022;32(18):2110931. doi:10.1002/adfm.202110931
18. Chen Y, Yu J, Ke Q, Gao Y, Zhang C, Guo Y. Bioinspired fabrication of carbonated hydroxyapatite/chitosan nanohybrid scaffolds loaded with TWS119 for bone regeneration. *Chem Eng J*. 2018;341:112–125. doi:10.1016/j.cej.2018.02.010
19. Shakir M, Jolly R, Khan AA, et al. Resol based chitosan/nano-hydroxyapatite nanoensemble for effective bone tissue engineering. *Carbohyd Polym*. 2018;179:317–327. doi:10.1016/j.carbpol.2017.09.103
20. Su Y, Li K, Tielens F, Wang J. Effect of sprayed techniques on the surface microstructure and in vitro behavior of nano-HAp coatings. *Mat Sci Eng C-Mater*. 2020;117:111318. doi:10.1016/j.msec.2020.111318
21. Shi FN, Almeida JC, Helguero LA, Fernandes MH, Knowles JC, Rocha J. Calcium phosphonate frameworks for treating bone tissue disorders. *Inorg Chem*. 2015;54(20):9929–9935. doi:10.1021/acs.inorgchem.5b01634
22. Nazeer MA, Yilgor E, Yilgor I. Intercalated chitosan/hydroxyapatite nanocomposites: promising materials for bone tissue engineering applications. *Carbohyd Polym*. 2017;175:38–46. doi:10.1016/j.carbpol.2017.07.054
23. Zhang J, Liu G, Wu Q, Zuo J, Qin Y, Wang J. Novel mesoporous hydroxyapatite/chitosan composite for bone repair. *J Bionic Eng*. 2012;9(2):243–251. doi:10.1016/S1672-6529(11)60117-0
24. Zhou Y, Gao HL, Shen LL, et al. Chitosan microspheres with an extracellular matrix-mimicking nanofibrous structure as cell-carrier building blocks for bottom-up cartilage tissue engineering. *Nanoscale*. 2016;8(1):309–317. doi:10.1039/C5NR06876B
25. Leite ÁJ, Caridade SG, Mano JF. Synthesis and characterization of bioactive biodegradable chitosan composite spheres with shape memory capability. *J Non Cryst Solids*. 2016;432:158–166. doi:10.1016/j.jnoncrysol.2015.04.011
26. Chen D, Liu P, Li M, Zhang C, Gao Y, Guo Y. Nacre-mimetic hydroxyapatite/chitosan/gelatin layered scaffolds modifying substance P for subchondral bone regeneration. *Carbohyd Polym*. 2022;291:119575. doi:10.1016/j.carbpol.2022.119575
27. Tamer TM, Alsehli MH, Omer AM, et al. Development of Polyvinyl Alcohol/Kaolin Sponges Stimulated by Marjoram as Hemostatic, Antibacterial, and Antioxidant Dressings for Wound Healing Promotion. *Int J Mol Sci*. 2021;22(23):13050. doi:10.3390/ijms222313050
28. Kokubo T, Takadama H. How useful is SBF in predicting in vivo bone bioactivity? *Biomaterials*. 2006;27(15):2907–2915. doi:10.1016/j.biomaterials.2006.01.017
29. Nasirzade J, Alccayhuaman KAA, Kargarpour Z, et al. Acid dentin lysate failed to modulate bone formation in rat calvaria defects. *Biology*. 2021;10(3):196. doi:10.3390/biology10030196
30. Zimina A, Senatov F, Choudhary R, et al. Biocompatibility and Physico-Chemical Properties of Highly Porous PLA/HA Scaffolds for Bone Reconstruction. *Polymers*. 2020;12(12):2938. doi:10.3390/polym12122938

31. Wu J, Li G, Ye T, et al. Stem cell-laden injectable hydrogel microspheres for cancellous bone regeneration. *Chem Eng J*. 2020;393:124715. doi:10.1016/j.cej.2020.124715
32. Liu S, Zhou C, Mou S, et al. Biocompatible graphene oxide-collagen composite aerogel for enhanced stiffness and in situ bone regeneration. *Mat Sci Eng C-Mater*. 2019;105:110137. doi:10.1016/j.msec.2019.110137
33. Iglesias-Mejuto A, Garcia-Gonzalez CA. 3D-printed, dual crosslinked and sterile aerogel scaffolds for bone tissue engineering. *Polymers*. 2022;14 (6):1211. doi:10.3390/polym14061211
34. Jalota S, Bhaduri SB, Tas AC. Effect of carbonate content and buffer type on calcium phosphate formation in SBF solutions. *J Mater Sci Mater Med*. 2006;17(8):697–707. doi:10.1007/s10856-006-9680-1
35. Banerjee S, Bagchi B, Bhandary S, et al. Antimicrobial and biocompatible fluorescent hydroxyapatite-chitosan nanocomposite films for biomedical applications. *Colloids Surf B Biointerfaces*. 2018;171:300–307. doi:10.1016/j.colsurfb.2018.07.028
36. Ke CL, Deng FS, Chuang CY, Lin CH. Antimicrobial Actions and Applications of Chitosan. *Polymers*. 2021;13(6):904. doi:10.3390/polym13060904
37. Iglesias-Mejuto A, Garcia-Gonzalez CA. 3D-printed alginate-hydroxyapatite aerogel scaffolds for bone tissue engineering. *Mat Sci Eng C-Mater*. 2021;131:112525. doi:10.1016/j.msec.2021.112525
38. Ladeira BMF, Gomes MC, Custodio CA, Mano JF. High-Throughput Production of Microsponges from Platelet Lysate for Tissue Engineering Applications. *Tissue Eng Part C Methods*. 2022;28(7):325–334. doi:10.1089/ten.tec.2022.0029
39. Dai Y, Gao Z, Ma L, Wang D, Gao C. Cell-Free HA-MA/PLGA Scaffolds with Radially Oriented Pores for In Situ Inductive Regeneration of Full Thickness Cartilage Defects. *Macromol Biosci*. 2016;16(11):1632–1642. doi:10.1002/mabi.201600218

International Journal of Nanomedicine Dovepress

Publish your work in this journal

The International Journal of Nanomedicine is an international, peer-reviewed journal focusing on the application of nanotechnology in diagnostics, therapeutics, and drug delivery systems throughout the biomedical field. This journal is indexed on PubMed Central, MedLine, CAS, SciSearch®, Current Contents®/Clinical Medicine, Journal Citation Reports/Science Edition, EMBase, Scopus and the Elsevier Bibliographic databases. The manuscript management system is completely online and includes a very quick and fair peer-review system, which is all easy to use. Visit http://www.dovepress.com/testimonials.php to read real quotes from published authors.

Submit your manuscript here: https://www.dovepress.com/international-journal-of-nanomedicine-journal